AGU PUBLICATIONS

JGR

Journal of Geophysical Research: Space Physics

RESEARCH ARTICLE
10.1002/2014JA020258

Key Points:
- Investigate effect of compressional waves launched from rotating current sources
- A range of observed periodic phenomena is controlled by compressional waves
- Our model predicts dawn-dusk asymmetry of the magnetopause boundary

Correspondence to:
M. Kivelson,
mkivelson@igpp.ucla.edu

Citation:
Kivelson, M. G., and X. Jia (2014), Control of periodic variations in Saturn's magnetosphere by compressional waves, *J. Geophys. Res. Space Physics*, *119*, 8030–8045, doi:10.1002/2014JA020258.

Received 5 JUN 2014
Accepted 8 SEP 2014
Accepted article online 11 SEP 2014
Published online 1 OCT 2014

Control of periodic variations in Saturn's magnetosphere by compressional waves

Margaret Galland Kivelson[1,2] and Xianzhe Jia[1]

[1]Department of Atmospheric, Oceanic, and Space Sciences, University of Michigan, Ann Arbor, Michigan, USA, [2]Department of Earth, Planetary, and Space Sciences, University of California, Los Angeles, California, USA

Abstract Many of the periodic variations observed in Saturn's magnetosphere can be linked directly to the presence of a rotating pattern of field-aligned currents that link the northern and southern ionospheres with each other and with the magnetosphere. Such a current system is incorporated in a magnetohydrodynamic simulation that has previously been shown to reproduce many of the observed periodic properties of the system. Here the simulation is used to investigate a range of phenomena that can be attributed to the effects of compressional waves launched from the rotating current sources. The compressional waves are found to drive the flapping of the plasma sheet and the expansion and contraction of the magnetopause in each rotation period. Because the compressional perturbations weaken as they rotate from morning to evening around the dayside of the magnetosphere, the boundary develops a strong morning-evening asymmetry. A fit to the shape is provided that may be useful in further investigation of magnetopause properties, but there is already evidence of the proposed asymmetry in the observations of Clarke et al. (2010a).

1. Introduction

Periodic variations at roughly Saturn's rotation period were first identified in the power emitted in kilometric radiation (SKR) [*Desch and Kaiser*, 1981; *Gurnett et al*., 2005; *Kurth et al*., 2007, 2008; *Lamy*, 2011]. Subsequent studies have found the periodicity of SKR in diverse features of the magnetosphere including the perturbation magnetic field near the equator [*Andrews et al*., 2008, 2010a, 2010b], the flapping of the equatorial current sheet [*Khurana et al*., 2009; *Arridge et al*., 2011], the location of the magnetopause and bow shock [*Clarke et al*., 2006, 2010a, and 2010b], the plasma density [*Gurnett et al*., 2007], the intensity of energetic neutral atom fluxes [*Paranicas et al*., 2005; *Carbary et al*., 2008], and auroral properties [*Nichols et al*., 2008, 2010; *Provan et al*., 2009; *Carbary*, 2013]. The source of the periodicities remains uncertain, but there is little doubt that field-aligned currents (FACs) are required to couple the rotating planet to the equator and to impose periodic behavior on the entire system. The rotating FACs drive rather directly such magnetospheric signals as magnetic perturbations inside of ~15 R_S (R_S = 60268 km is Saturn's radius) and SKR emissions that rotate about the planet. However, other phenomena, including plasma sheet flapping and magnetopause motion, although periodic, do not rotate. These types of responses require the rotating current system to couple to compressional perturbations that can drive nonrotational periodic behavior, a different mode of magnetospheric response. In this work we focus on compressional signals that drive reconfiguration of the magnetosphere, displace the plasma sheet of the magnetotail, and control the location and shape of the magnetopause.

The results presented here are based on a magnetohydrodynamic (MHD) simulation that introduces the periodicity through a heuristic pattern of FACs rotating at a prescribed period. In the model, the FACs that link the ionosphere and the magnetosphere are driven by vortical flows imposed on the ionosphere [*Jia et al*., 2012; *Jia and Kivelson*, 2012], but the driver of the vorticity is unspecified. The flow pattern could arise through coupling to vortical winds in the thermosphere such as have been explored by *Smith* [2006, 2010] or through perturbations of polar cap rotation such as those proposed by *Southwood and Cowley* [2014]. However they are imposed, we argue that the dynamo source of the currents must have sufficient inertia to restore both periodicity and phase of the perturbations subsequent to intermittent magnetospheric reconfigurations driven by the solar wind. We, therefore, argue that the source is likely to involve the thermosphere either as source or flywheel. The simulation captures numerous properties imposed by ionosphere-magnetosphere coupling with considerable fidelity. Here we continue to explore its properties in order to understand better some of the more puzzling features of the observations not previously examined (e.g., by *Jia et al*. [2012] and *Jia and Kivelson* [2012]).

The version of the simulation used in this analysis is presented in *Jia et al.* [2012], which should be consulted for details. Critical to understanding this paper are the following features: The planetary dipole (equatorial surface strength of 20,800 nT) is centered, implying internal north-south symmetry of background properties. The inner boundary of the simulation is a sphere at 3 R_S. The solar wind is maintained constant throughout the simulation. It flows at 400 km/s at right angles to the spin axis in the $-X$ direction. Its density and temperature are 0.05 amu/cm^3 and 20 eV, respectively. The dynamic pressure is thus 0.013 nPa. The interplanetary magnetic field (0.5 nT) is oriented southward, and there is no evidence of reconnection at the dayside boundary. Periodicity is imposed in the southern ionosphere where a pair of flow vortices, centered at 70° southern latitude, rotates rigidly at the nominal 10.8 h period of modulation of the southern SKR signal close to southern summer solstice in the early part of the Cassini mission [*Gurnett et al.*, 2005; *Kurth et al.*, 2007, 2008; *Lamy*, 2011]. The vortices drive FACs into the magnetosphere and, in part, to the opposite ionosphere. The interhemispheric currents form what has been described as a rotating cam current system [*Southwood and Kivel*son, 2007].

Section 2 describes the compressional perturbations that arise in the equatorial magnetosphere and notes that they do not rigidly rotate with the ionospheric current sources, especially in regions beyond ~15 R_S. Section 3 describes the compressional perturbations as waves and characterizes their properties. The effects of the waves on the dayside boundaries and on the nightside plasma sheet are noted. Section 4 provides more quantitative insight into the periodic displacement of the modeled magnetopause and discusses the structure and location of the nightside plasma sheet. Section 5 explains why the maximum magnetopause displacement is found at a different rotation phase in observations and in the simulation. Section 6 provides a model of the dawn-dusk asymmetry of the magnetopause boundary and characterizes its variation with rotation phase. Section 7 relates the magnetopause displacement to the periodic flow bursts or plasmoids that form in the simulation. Section 8 identifies features of our predictions that can be tested with Cassini data.

2. Compressional Signals

Compressional perturbations are observed in numerous properties of Saturn's magnetosphere including the magnitude of the magnetic field, the plasma density and pressure, and the magnetic pressure [*Andrews et al.*, 2010a, *Ramer et al.*, 2013]. In the MHD simulation, the periodicity imposed by ionospheric sources results in significant periodic reconfiguration of the entire magnetosphere. In order to understand how such variations are imposed by localized current sources, we examine the development and propagation of periodically varying compressional signals. At each position in the simulation volume, we average over five rotation periods to obtain the rotation-averaged thermal pressure, magnetic pressure, and total pressure ($<P_{\rm th}>$, $<P_b>$, $<P_{\rm thb}> = <P_{\rm th}> + <P_b>$); we define the perturbations ($dP_{\rm th}$, dP_b, $dP_{\rm thb}$) as the differences between values at a specific simulation time and the calculated averages.

Figure 1 gives examples of the spatial variation of pressure perturbations at different rotation phases. The columns (from left to right) show perturbations of thermal pressure, magnetic pressure, and their sum in the equatorial plane. Rows are separated by 2 h or 19% of a rotation period within a single rotation period. In each equatorial plot, a contour marked by small green circles delineates the equatorial crossing of the magnetic shell at 70° invariant latitude, from which field lines have been traced every 10° of longitude in the ionosphere. (In the simulation, the rotating ionospheric vortices that drive FACs are centered on 70° south latitude.) Unit vectors show the direction of the magnetic perturbations imposed by the rotating FACs. Orange curves identify the locus of the magnetopause identified as the last closed field line.

We refer to the magnetic perturbations inside of ~12–15 R_S as the "cam field," alluding to the descriptions of the quasi-uniform perturbation field in the middle magnetosphere given by *Southwood and Kivelson* [2007] and *Andrews et al.* [2008]. The quasi-uniform field (arrows in the diagrams) rotates; its orientation correlates with the intensity of SKR emissions. The magnetic pressure perturbations (column 2) reveal that a field-aligned component of the cam field is present. Near the equator, the average magnetic field (**B**) orientation is southward, with $B_\theta > 0$. Correspondingly, positive magnetic pressure perturbations imply positive dB_θ. For a source in the Southern Hemisphere, the field-aligned perturbation is known to vary in phase with the radial component [*Andrews et al.*, 2010a; *Provan et al.*, 2009] and the same is true of the simulation. The magnetic pressure perturbations are closely coupled to rotation phase inside of ~15 R_S. For example, at hour 194,

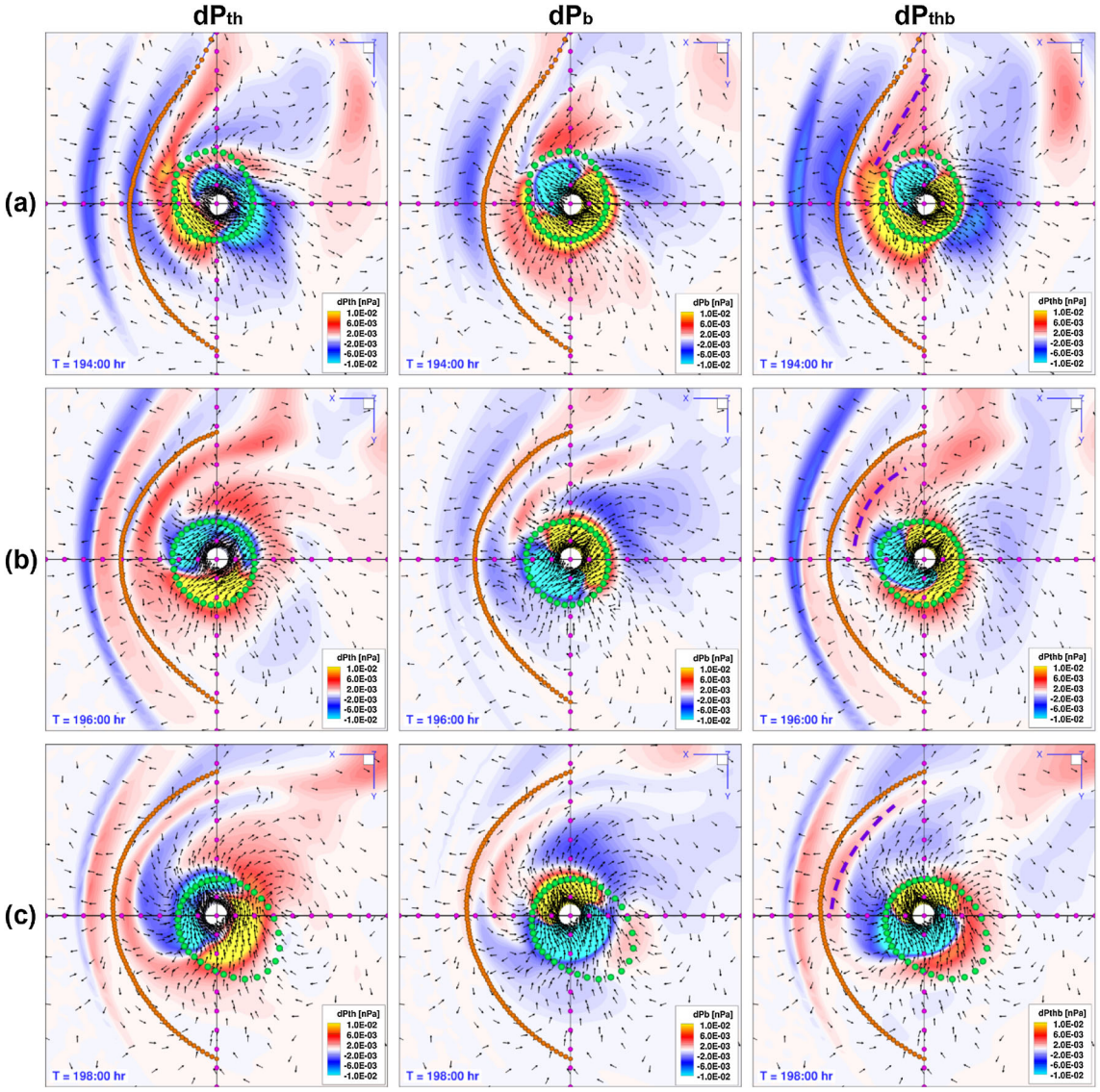

Figure 1. Equatorial plane perturbations (the Sun is at the left) extracted from the *Jia et al.* [2012] MHD simulation of periodic variations in Saturn's magnetosphere. The Sun is to the left. Plots are extracted at hours (a) 194, (b) 196, (c) 198, (d) 200, (e) 202, and (f) 204. Magenta circles on the axes are separated by 5 R_S. (left to right) Color bars represent the change of perturbation thermal pressure, magnetic pressure, and total pressure. The color scales correspond to a pressure range of ±0.01 nPa. In the plots of total pressure perturbations, we have overlaid purple dashed curves to identify the peak positive perturbations at different time steps so that their displacements at successive time steps become more apparent. Arrows are unit vectors in the direction of the perturbation magnetic field. Green circles lie on the 70° invariant latitude shell starting in the ionosphere with 10° of azimuthal separation. The orange contour is the magnetopause extracted from the simulation as the open-closed field line boundary.

inside of 15 R_S positive dP_b is centered at about 2130 LT and negative dP_b is centered roughly 12 h later in LT, near 0930. A rigidly rotating perturbation would move through ~4.5 h of LT in 2 h, displacing the center of the positive perturbation to ~0200 LT at hour 196 in Figure 1b, to ~0630 LT at hour 198 in Figure 1c, and so forth. The center of the negative perturbation would remain in antiphase with the positive perturbation. The plots confirm these expectations and are consistent with the assumption of nearly rigid rotation in the inner and middle magnetosphere where Cassini magnetometer measurements have been analyzed [*Andrews et al.*, 2010a; *Provan et al.*, 2009]. The assumption of rigid rotation does not apply to the thermal pressure perturbations even in the inner region. The form of the perturbation varies with rotation phase, with peak and trough changing relative phase through a cycle. For example, minima of thermal pressure perturbations (Figure 1a, column 1) are present at two different local times and radial distances in the inner magnetosphere. Neither of them is 12 h away from the local time of the maximum.

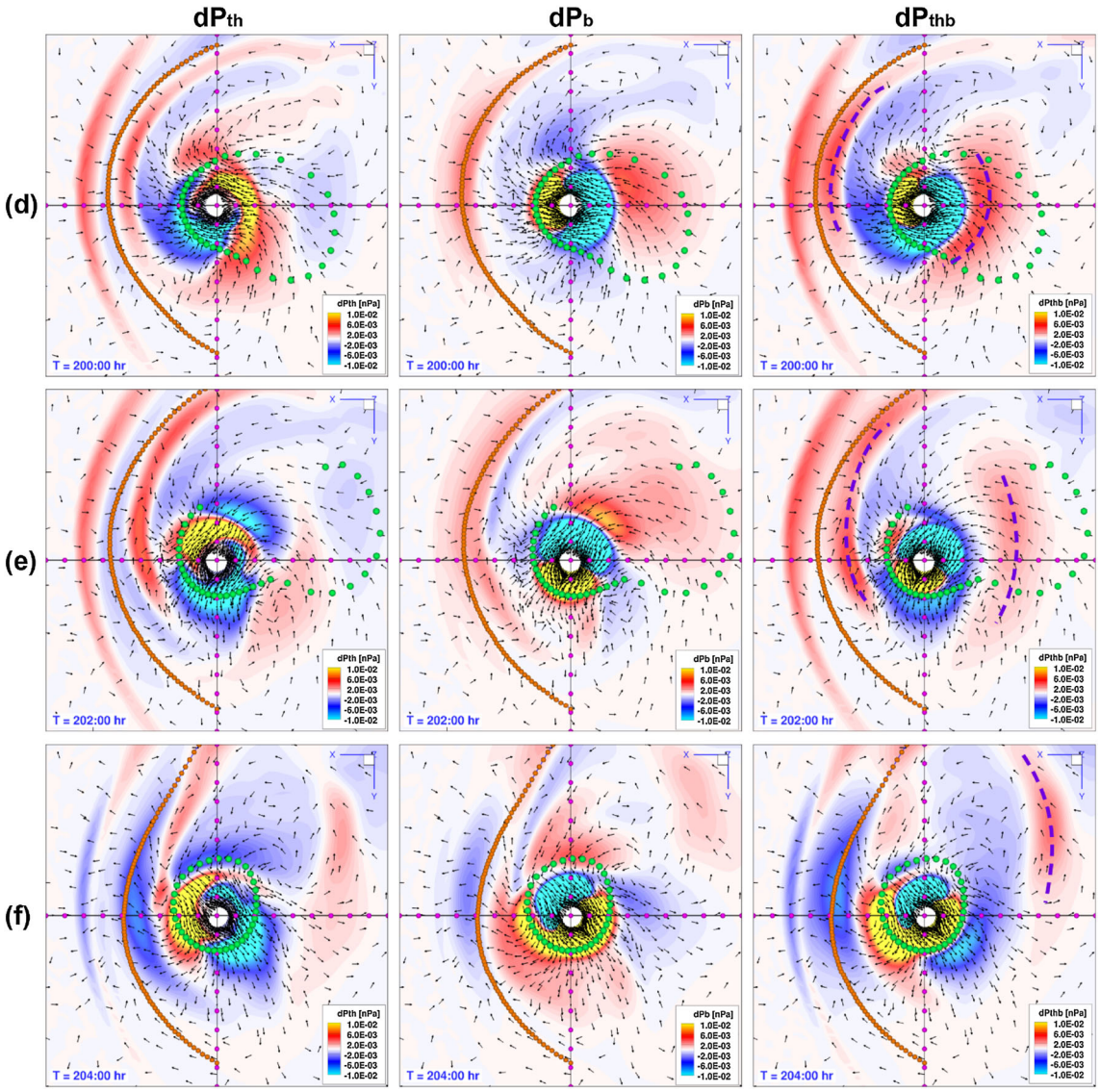

Figure 1. (continued)

Although increases and decreases of pressure perturbations rotate through local time inside of ~15 R_S, even if not rigidly, the temporal evolution of pressure perturbations is far from purely rotational outside of ~15 R_S. In this outer region, compressional structures behave like waves moving not only azimuthally but also radially outward. Evidently, the picture of purely rotating perturbations is not systematically valid. We discuss the propagation and the effect of compressional waves in subsequent sections.

3. Propagating Pressure Fronts

The properties of the solar wind in the simulation remain fixed. Consequently, pressure perturbations launched by the rotating FACs of our MHD model and propagating sunward on the dayside cause the magnetopause and bow shock to move and change form. On the nightside, the pressure perturbations propagating tailward modify the structure and position of the current sheet. Throughout the outer magnetosphere, the pressure perturbations have the form of propagating waves.

The shifting locations of pressure fronts in successive plots of Figure 1 allow us to estimate the equatorial radial component of the group velocity of the waves that change the global structure. For example, near midnight in Figure 1d at hour 200, the total pressure peak (red and emphasized with a dashed purple curve)

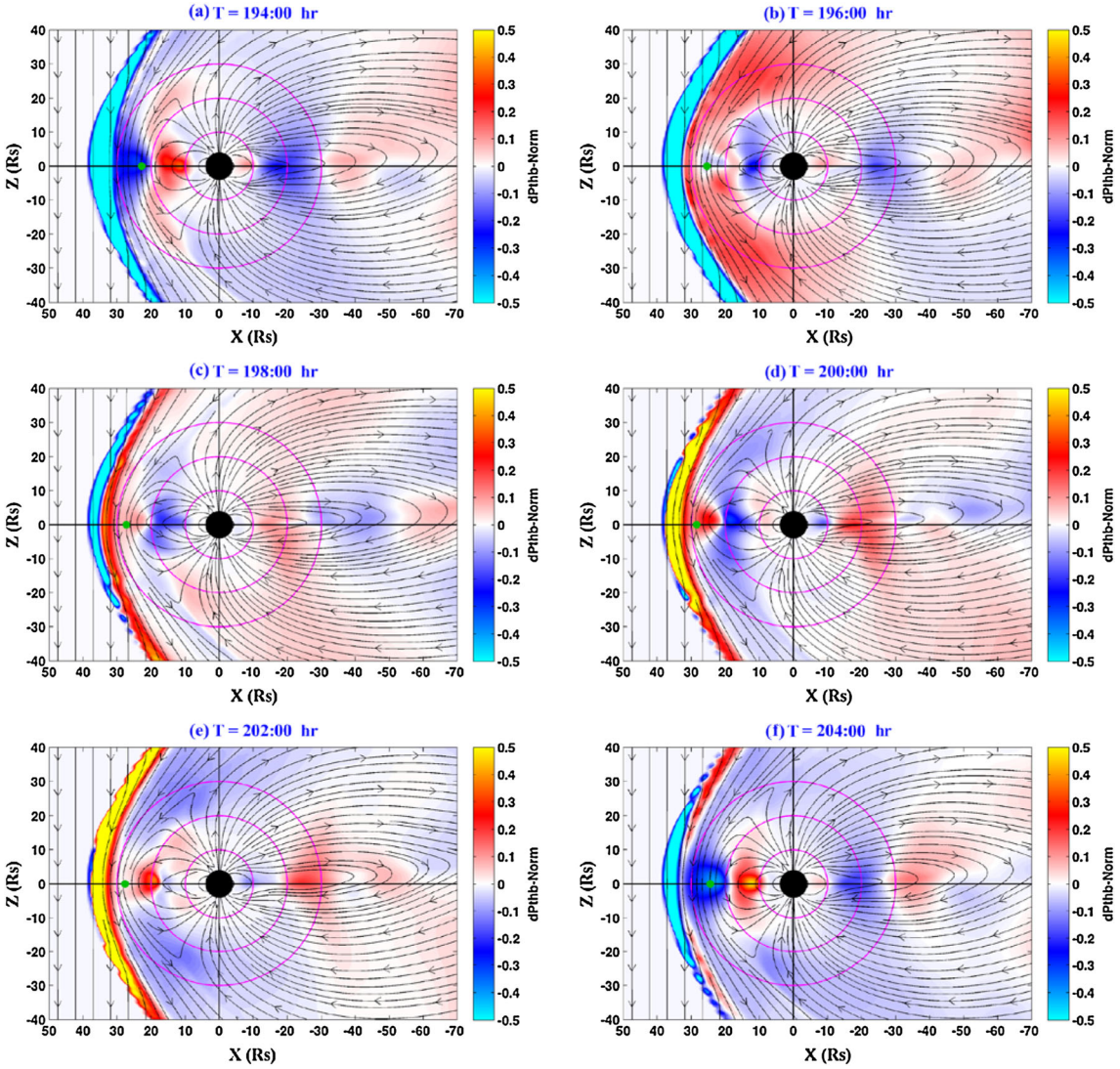

Figure 2. (a–f) Pressure perturbations (dP_{thb}) normalized to the average background pressure ($<P_{thb}>$) in the noon-midnight meridian plane are shown in color at times differing by 2 h between hours 194 and 202 in the simulation. The Sun is to the left. Black curves are field lines selected for approximately uniform coverage and projected into the meridian plane. The small green circles show the location of the nose of the magnetopause. The magenta circles have radii of 10, 20, and 30 R_S. The central black circle has a radius of 4 R_S.

is centered just beyond 15 R_S. At hour 202, in Figure 1e, the total pressure enhancement has rotated to later local time and moved radially outward near midnight to about 23 R_S. At hour 204 (Figure 1f), the perturbation has rotated to still later local time and is centered near 33 R_S, implying outward propagation by 60–100 km/s or ~1 R_S in 10 min, implying that displacements may propagate further than 50 R_S downtail within a rotation cycle. On the dayside, the waves appear to move mostly azimuthally with smaller radial velocity.

The sense of radial propagation of the compressional waves beyond ~ 15 R_S changes through a rotation period. Even in the widely spaced time steps of Figure 1, the propagation of the fronts in dP_{thb} can be followed. On the dayside, a compressional perturbation in the prenoon sector moves outward, starting in Figure 1a and continuing in Figures 1b–1d. In Figure 1e the front begins to retreat inward and has disappeared in Figure 1f. Wavelengths of waves propagating radially on the dayside are of order 5–10 R_S. On the nightside, fronts propagate downtail with wavelengths of order 35 R_S. Simulation steps not illustrated confirm that inward and outward propagation is occurring as inferred from the time steps shown in Figure 1.

A cut through the noon-midnight meridian plane (Figure 2) reveals additional features of the compressional waves that propagate through the system at the same time steps as those selected for Figure 1. Because the

background field varies by orders of magnitude over the range of distances plotted, we have normalized the pressure perturbation to the background pressure; thus, in these plots, color represents $dP_{thb}/<P_{thb}>$. On the nightside, the pressure peaks and troughs in the south are typically slightly more intense and more widely distributed than they are in the north. For example, tailward of ~10 R_S in Figures 2c and 2d, the red region (positive pressure perturbation) is brighter and more extended in the south than in the north, and in Figures 2a and 2f the blue region (negative pressure perturbation) is brighter and more extended in the south than in the north. Centers of the extrema of pressure perturbations move at an angle of ~6° northward as they propagate down the tail and drive north-south displacements of the tail plasma sheet. This northward drift is seen best by following the pressure minimum (blue) seen near $x = -20$ R_S in Figure 2a, in the region -30 to -40 R_S in Figure 2c, and beyond -40 R_S in Figure 2d. The center of the plasma sheet (defined for this purpose by the reversal of B_r) remains slightly northward of the equator through the entire rotation period illustrated. Focusing on the region near $X = -20$ R_S, we find that the center of the plasma sheet falls closest to the equator at hour 196, following the passage of a reduced pressure front and farthest above the equator at hour 200 as a front of increased pressure passes.

The stationary boundary on the upstream side in Figure 2 corresponds to the location of the bow shock at its extreme excursion. When the bow shock lies closer to Saturn, the pressure perturbation about the mean is negative just inside the upstream boundary. The boundary is displaced farthest inward at hour 194 when a minimum of pressure perturbation is present over several R_S inside the extremum of the bow shock location. At hour 196, a positive pressure perturbation in the outer magnetosphere initiates outward motion of the boundary. The positive pressure perturbation remains present for several hours. Within the outermost boundary, the pressure perturbation is predominantly positive when the outward displacement is greatest at hours 200 and 202. At hour 204, a minimum in pressure is seen in the region within the extremum of the bow shock location and the boundary has moved back in.

In a uniform field, compressional MHD waves that propagate rapidly across the background field are fast-mode waves; such waves have a predictable in-phase relation between magnetic and thermal pressure. It is initially perplexing to note that the perturbations of magnetic and thermal pressure shown in Figure 1 are more often in antiphase than in phase, but in a nonuniform system, fast- and slow-mode waves are coupled, and the simple relations between magnetic and thermal pressure perturbations no longer apply. For example, an out-of-phase relationship may arise if the thermal pressure distribution falls off with radial distance at a faster rate than the adiabatic pressure lapse rate. Rotation further complicates the picture. For example, where rotating flux tubes are stretched outward, reducing B_θ in the equatorial region, centrifugal acceleration drives plasma along the flux tube toward the equator, readily accounting for the antiphase perturbations observed in the figure. It follows that the phase relations between variations of thermal and magnetic pressure are unpredictable in a nonuniform magnetic field in a rotating plasma.

The periodic pressure variations that we analyze here are initiated by the rotating flows that we imposed on the ionosphere. The associated magnetic perturbations can be followed through the noon-midnight meridian in Figure 3. The rows of the figure are separated by 2 h and are taken at the times selected for Figures 1 and 2. The columns (left to right) show the components of the magnetic perturbations, with the transverse toroidal and meridional components in the first two columns and the field-aligned component in the third column. The striking new information in this set of images is the relation of the magnetic perturbations to the sources of the FACs in the southern ionosphere. The centers of the ionospheric vortices at 70° latitude lie in the meridian plane at hours ~197 and ~202. The azimuthally extended sheet currents that flow out of or into the ionosphere near the centers of the vortices (in opposite senses near noon and near midnight) account for the strong toroidal perturbations emerging from high latitude in the southern ionosphere (bright yellow and cyan regions emerging from the black circle) at hours 196 and 198 and at hours 202 and 204. In the noon meridian, the positive perturbation is on the high-latitude side; and in the midnight meridian, it is on the low-latitude side of the extended signal, as required for oppositely directed field-aligned current sheets in the two sectors. The breaks between the clockwise and counterclockwise ionospheric vortices lie in the noon-midnight meridian plane at hours ~194 and ~199:30. At times near these rotation phases (hours 194–196 and 200), the predominantly latitudinal ionospheric flows impose intense meridional perturbations in the Southern Hemisphere, which are apparent in the figure as yellow and cyan regions emerging from the black circle in the plot of the poloidal component of the perturbation. The reversal

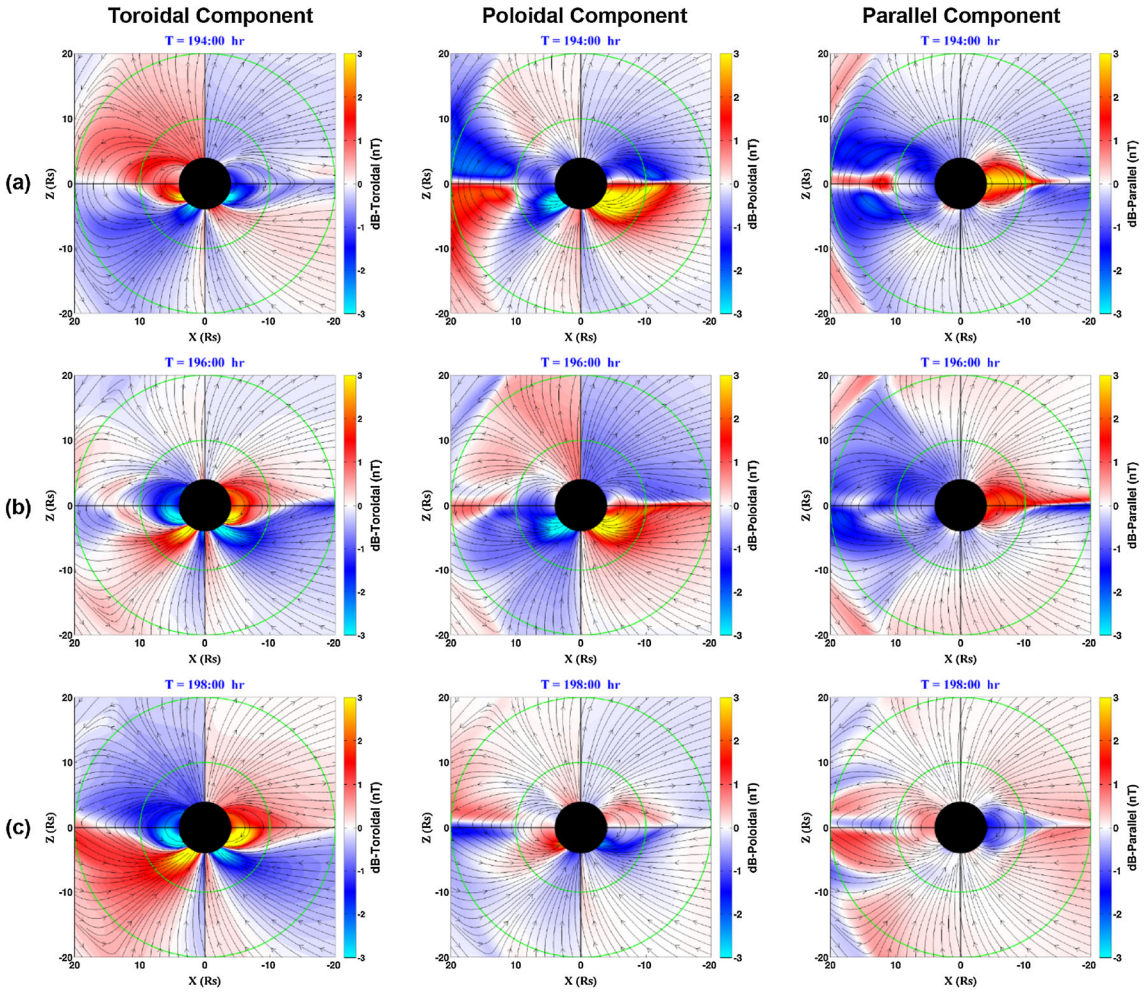

Figure 3. Noon midnight meridian cuts at time steps within a rotation cycle as in Figure 1. (left) Transverse azimuthal components. (middle) Transverse meridional components of the perturbation magnetic field. (right) Field-aligned components of the magnetic field. Perturbations are differences between the instantaneous magnetic field and the magnetic field averaged over 5 cycles, with values in nT indicated on the color scale. Green circles have radii of 10 and 20 R_S. The black circle has a radius of 4 R_S.

of the meridional transverse perturbation approximately across the equatorial plane (note the change of color across the equator on the nightside at these times) shows that the nightside current sheet is twisted at an angle relative to the equatorial plane.

The right-hand column of Figure 3 shows field-aligned perturbations, which are less intense than the transverse perturbations but central to the large-scale motions of the magnetosphere that we are trying to understand. They, too, arise from the flows imposed by the ionospheric vortices, flows directed meridionally at locations 90° from the centers of the vortices (in the noon-midnight meridian plane at hours 194 and 200, for example), and directed zonally near the centers of the vortices (near the noon-midnight meridian plane at hours 196 and 198, for example). Meridional flows in the ionosphere compress or expand the field and drive the weak field-aligned perturbations seen near the southern sources on the right at hours 194 (positive perturbation near noon and negative perturbation near midnight) and 200 (negative perturbation near noon and positive perturbation near midnight). Close to the planet, normalized compressional components of the perturbation field are negligible because of the rigidity of the background field, but the perturbations become significant where the background field drops below of order tens of nT. Thus, the most intense field-aligned component of the normalized perturbation field is concentrated near the equator. Inside of ~15 R_S the compressional perturbations are typically in phase with the meridional perturbations in the Southern Hemisphere in the same local time sector, as expected from the effects of latitudinal flows imposed by the ionospheric vortices, and also in phase with the magnetic pressure perturbations to which they contribute.

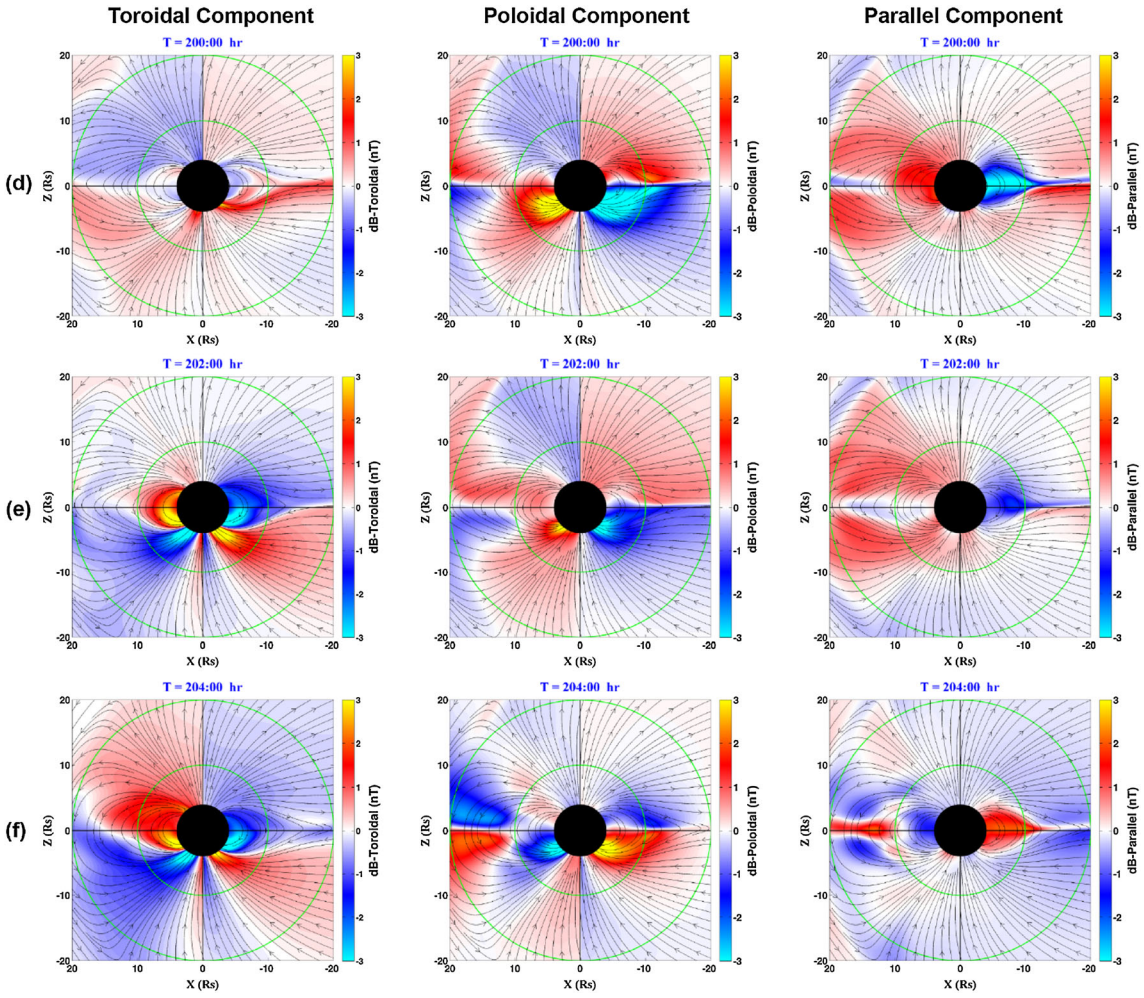

Figure 3. (continued)

4. Magnetopause and Plasma Sheet Motion

Figure 1 is helpful in identifying the large-scale oscillation of the magnetopause. Orange curves represent the magnetopause identified as the open/closed field line boundary. A striking feature is the morning-evening asymmetry, a matter to which we will return. The solar wind conditions are steady and there is no evidence of dayside reconnection; but, over the rotation period, the magnetopause moves out and back in response to changing internal pressure. On the dayside, the pressure fronts propagate right through the magnetopause. As expected in the MHD limit, the outward propagating pressure fronts do not modify the pressure in the solar wind. They merely cause the bow shock to move out and in. The excursions of the magnetopause are quantified in Figure 4, a plot of the distance to the subsolar magnetopause that reveals both the range of displacement—from ~23 R_S at hour 194 (and again at hour 204) to ~28 R_S at hour 200—and the nonsinusoidal nature of the motion. Comparison with Figure 1 shows that the greatest compression occurs about a quarter of a cycle before the SKR emissions would peak in the simulated magnetosphere.

Figure 1 confirms that the magnetopause is displaced by the propagating pressure fronts. When the nose of the magnetopause falls at a minimum radial distance along the noon meridian (e.g., Figure 1a, hour 194), it lies near a zero of dP_{thb} where pressure gradient forces vanish. However, an inward pressure gradient can be identified just inside the magnetopause, part of an outward propagating pressure perturbation that accounts for the outward motion of the boundary between hours 194 and 196 (Figures 1a and 1b). In the two succeeding time steps, the pressure boundary moves slowly outward while the pressure perturbations weaken. At maximum displacement near hour 200 (Figure 1d), the nose of the magnetopause again lies close to a zero in pressure perturbation where it continues to hover at hour 202 (Figure 1e). The sign of the

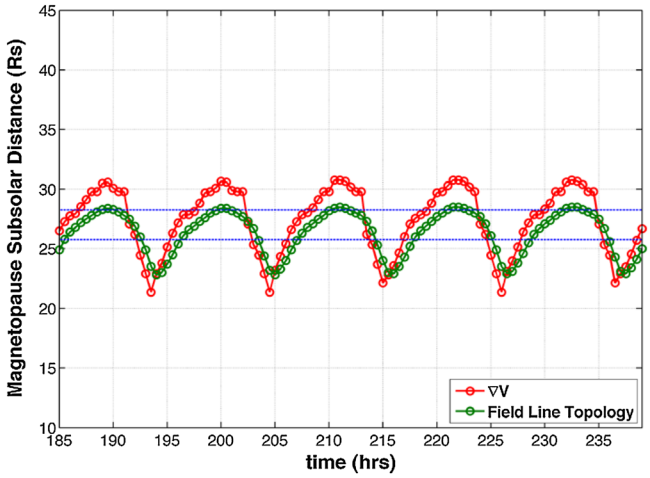

Figure 4. Location of the nose of the magnetopause as a function of simulation time. The red points identify the location of the largest velocity gradient. The green points identify the location of the open-closed field line boundary. The horizontal lines surrounding 27 R_S are separated by 2.5 R_S, marking the range of typical oscillations about the mean reported by *Clarke et al.* [2010b].

pressure perturbation near noon reverses between hours 202 and 204 (Figure 1f), consistent with the development of a reversed pressure gradient and inward motion of the magnetopause by about 3 R_S and completion of a cycle.

We have confirmed that the magnetopause is in approximate pressure balance in the model. The pressure along a portion of the *x* axis at hour 194, when the subsolar magnetopause lies at 23 R_S, and at hour 200 (when the subsolar magnetopause lies at 28 R_S) is plotted in Figure 5. The solar wind dynamic pressure remains constant at the nominal value of 0.013 nPa and quite closely matches the pressure at the boundary. Just within the boundary, the pressure perturbation slightly exceeds the solar wind dynamic pressure because part of the outward force per unit area is compensated by the curvature force. (The nonnegligible field curvature within the dayside boundary is evident in Figure 2.) Figure 5a shows a large inward gradient of the total pressure perturbation that accounts for the rapid outward displacement following hour 194 that is consistent with the gradient of the green curve in Figure 4. By contrast, at hour 200 when the magnetopause has reached its maximum displacement, the pressure gradient within the boundary (Figure 5b) is relatively small (once again probably partly compensated by curvature forces) and the rate of displacement of the boundary at this time step is very low, again consistent with the gradient of the green curve of Figure 4.

Although the phase-dependent changes of magnetic configuration are relatively subtle in regions dominated by the dipole field, at radial distances beyond ~15 R_S the entire magnetosphere changes its configuration periodically in response to the propagating pressure perturbations. In particular, compressional perturbations similar to those that we relate to the displacement of the magnetopause drive flows and reconfiguration of the plasma sheet on the nightside. The effects of the perturbations are particularly well revealed by the changing equatorial locus of the 70° invariant latitude shell shown in Figure 1. In Figure 1a, the equatorial intersection of this critical surface is approximately elliptical between ~10 and 15 R_S. In Figure 1b, roughly

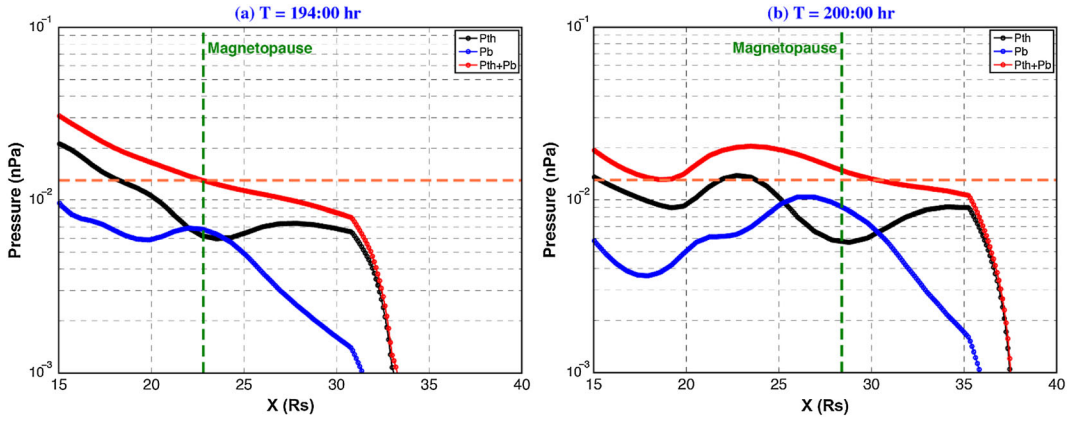

Figure 5. Plasma thermal pressure, magnetic pressure, and the total pressure (nPa) in the equatorial plane along the noon meridian plotted versus distance in R_S at hours (a) 194 and (b) 200 of the simulation. The dynamic pressure of the solar wind is represented by the dashed orange line. The location of the magnetopause is marked by the vertical green line.

coincident with SKR maximum, the distribution has contracted into a near circle of radius ~12 R_S. In Figure 1c, in a limited local time sector between dusk and midnight some of the green circles have moved out almost to 20 R_S. In Figure 1d, some of the circles in the premidnight sector have moved well beyond 30 R_S, and outward displacement has commenced in the postmidnight sector. In Figure 1e at a time close to SKR minimum, the most distant mapping is to a downtail distance beyond 40 R_S, and the peak outward displacement has rotated into the postmidnight sector. The significant outward displacements correspond to times when inward pressure gradients are propagating outward beyond $r \approx 12$ R_S on the nightside. For example, in Figures 1c and 1d (column 3), the perturbation pressure is high (red) inside and low (blue) outside of the outward moving boundary marked by the green circles on the nightside. In Figure 1e, the total pressure perturbation within the green circles is low. The boundary has reached its maximum displacement and has begun to contract to the form that it will have within 2 h following the start of the next cycle when the 70° invariant latitude boundary has contracted to resemble the form in Figure 1a. The maximum and minimum displacements of the 70° invariant latitude field lines on the nightside lag the maximum and minimum of outward displacements of the nose of the magnetopause by about 2 h, but to a good approximation, the entire magnetosphere appears to expand and contract over a cycle, changes described as "breathing" by *Ramer et al*. [2013].

The flows that displace the 70° invariant latitude shell indubitably relate to the processes that drive periodic plasmoid release in the simulation. Figure 8 of *Jia et al*. [2012] shows the structure of field lines that cross the equator at 20 R_S over an interval between hours 198 and 212, part of which overlaps the cycle selected for Figure 1. The structure at 20 R_S is highly ordered at hours 198 and 199. A bulge appears in the postmidnight sector at hour 100 and by hour 202; this bulge has developed into a large plasmoid that is centered high above the equatorial plane. The structure is largely gone by hour 206. The plasmoid moves upward off the equatorial plane in the next 4 h but does not disappear until hour 207 (a time that corresponds to approximately the same rotation phase as hour 197).

Because the background pressure is close to uniform throughout the tail, the plasma sheet is more readily identified in images showing the distribution of density than in the images of Figure 2 that show the distribution of normalized pressure perturbations. Images of density distributions and field lines through one cycle are shown in the simulation of *Jia and Kivelson* [2012] for a run in which a weak northern source is also included. Fortunately, the principal features of the variations are insensitive to the presence of the second signal, and there are only minor differences in response from one cycle to the next, so we can extract insight into the temporal variation of plasma sheet location from previously published figures. The comparison shows that the displacement of the plasma sheet from the equator occurs with increasing delay as a function of downtail distance. In the cycle illustrated in Figure 8 of *Jia and Kivelson* [2012], minimum magnetopause displacement occurs near hour 411; its position corresponds quite closely to that found at hour 194. Maximum magnetopause displacement occurs near hour 415:30 when the magnetopause lies close to 28 R_S. Responses in the magnetotail do not develop instantaneously. At minimum magnetopause compression (hour 411), the magnetotail current sheet falls on the equator between $0 > X > -45$ R_S. By hour 412:30, it has moved upward but only inside of -40 R_S. Both at hours 414 and 415:30 (the time of maximum displacement of the noon magnetopause), the tail current sheet lies well above the equator everywhere inside of -70 R_S. At hour 417, the inner part of the current sheet has moved back toward the equator but the region between -20 and -70 R_S is at its most northern extreme. The time delays are, of course, expected for the propagating compressional waves that we consider the source of the reconfiguration, and delays of the sort noted require propagation speeds close to 100 km/s, within a factor of 2 of the downtail speed in the near tail discussed in section 3.

Having noted that the tail expansion and contraction occur at different times at different locations, we must identify where we wish to examine the phenomenon of expansion and contraction. Let us consider the response of the plasma sheet in the region between $X = -10$ and -20 R_S. Before hour 415:30, Figures 8b and 8c of *Jia and Kivelson* [2012] show that the plasma sheet is compressed in the north-south direction. Near the time of maximum dayside expansion, the plasma sheet is relatively thick in the same region as seen in Figures 2e and 2f. This response is what leads us to describe the magnetosphere as expanding and contracting, even though the responses are not observed instantaneously at all locations.

5. Relation of Simulated to Observed Magnetopause Motion

The compressional perturbations identified in section 3 drive the periodic excursions of the dayside magnetopause that we characterized in section 2. The pressure fronts appear to rotate from morning to evening and in most of the panels in Figure 1, the perturbations weaken as they rotate past noon. This change is reflected in the boundary position which is found to have a significant morning-evening asymmetry, lying closer to Saturn on the evening side.

In this section, we compare the properties of the boundary extracted from the simulation with properties of the magnetopause inferred from Cassini data by *Clarke et al*. [2006, 2010a]. *Clarke et al*. [2010a] find typical oscillations of order 1.2 R_S about the mean, but note that some of the displacements are as great as ~4–5 R_S. The shape of the curves in Figure 4, representing the radial distance to the nose of the magnetopause extracted from the simulation, explains the two ranges. The simulated displacement varies nonsinusoidally. Encounters near noon would occur somewhere near 27 R_S for 70% of all random crossings (within the upper and lower bounds of the horizontal lines in the figure) for the assumed solar wind dynamic pressure. On 30% of all random crossings, inward displacements to 23 R_S would account for the report of occasional motion through as much as 4–5 R_S. The range of displacements differs at other local times, but even away from noon, the interpretation in terms of the nonsinusoidal structure of the curves provides a basic understanding of the statistics of observed magnetopause encounters.

Although the position of the magnetopause and its range of displacement are well represented in the simulation, the timing of the maximum and minimum displacements relative to the rotation phase of the core field is not. Let us try to understand why there is such a discrepancy of phase. In order to compare with observations, we note that the orientation of the magnetic perturbations inside of ~15 R_S provides the effective SKR phase. In the "longitude" system defined by *Kurth et al*. [2008], the most intense SKR emissions occur, on average, "when the subsolar longitude is 100°, as was the case in the Voyager era." For the interval from October 2004 to July 2006, *Andrews et al*. [2008], following the orientation of the cam field, establish that "at the peak of the SKR modulation, the field points radially outward (and southward) at ~0200 LT ± 2 h," a location at which the SKR *phase* (a nomenclature that we prefer to *longitude*) is 250°. *Clarke et al*. [2010a] report that the maximum outward displacement of the magnetopause occurs when the cam field (within ~15 R_S) points away from the dayside (>250° phase), but Figure 1 shows that the magnetopause displacement maximizes when the cam field points toward the dayside (~100° phase).

In the simulation, the magnetopause location is modulated by compressional waves launched from a source region near 12 R_S. If the wave speeds in the simulation are underestimated in the region beyond ~10–15 R_S, there will be a delay in the magnetopause response. *Clarke et al*. [2010a] infer radial wave speeds of 250 km/s on the dayside. In this region, the simulated wave speed varies through a rotation period from less than 50 km/s to ~200 km/s, with brief and localized occurrence of higher speeds. Beyond ~11 R_S, the mean wave speed is roughly 100 km/s and less than half that speed is radially directed.

We can explain why compressional wave speeds are underestimated in the simulation. The difference between the measured and modeled radial wave speeds (250 km/s versus ~50 km/s) results from the fact that MHD simulations do not include the effects of superthermal plasma. Where the pressure of energetic particles is important, the fast-mode wave speed is underestimated. In Saturn's magnetosphere, the thermal plasma dominates the pressure within 11 R_S. In that part of the magnetosphere, we believe that signal propagation speed is well represented in the simulation. Energetic particles contribute significantly to the thermal pressure beyond that distance [*Sergis et al*., 2010], so in the outer part of the magnetosphere, the processes linked to the imposition of periodic perturbations may be captured by the simulation but timing may be inconsistent with observations. A linear approximation to the Sergis et al. plot of total pressure in units of nPa in Figure 1b is $P(10^{-10}\ \mathrm{Pa}) = 4.625 - 0.275\ r(R_S)$, with average from 11 to 21 of 3.25 a factor of 16.3 larger than the average pressure found in this region in the MHD simulation. The difference between modeled and observed phases can be understood if the (missing) energetic particle pressure exceeds the thermal pressure by a factor of ~16 in the outer magnetosphere. Wave speeds are proportional to the square root of the pressure, so the wave speed in the simulation is reduced by roughly a factor of 4, close to the factor of 5 estimated above. A wave traveling radially outward at 250 km/s requires 40 min to travel 10 R_S. The simulated waves in the outer magnetosphere require 2 h and 40 min to propagate 10 R_S and only part of

that is radial propagation. Waves propagating at 45° to the radial direction would cover the distance in half a cycle. We believe that this slow outward expansion of compressional perturbations accounts for the delay in the time of maximum outward displacement of the magnetopause in the simulation.

One may ask whether the failure to incorporate effects of the high-pressure population in the simulation affects results other than propagation speeds. We emphasize that the effects of neglecting the energetic particle population may affect not only wave phase velocities but also other results of the model that we have not explicitly identified. Furthermore, an MHD simulation does not correspond to properties of the actual magnetosphere in other ways. Numerical dissipation in the simulation, for example, is likely to exceed dissipation in the Saturn system, and it is hard to identify how this affects our results. The simulation does not model pressure anisotropy, which can be important in regions where ion pickup rates are high. Consequently, the simulated plasma density is underestimated near the equator and overestimated off the equator, particularly on L shells between 4 and 10. On the other hand, the flux tube content is more correctly represented because of careful selection of simulation parameters. Thus, we recognize that the model magnetosphere is not fully faithful as a representation of Saturn's magnetosphere. However, the amplitude of the periodic perturbations seems to be well modeled. This is largely because the periodicities are driven by FACs, and the locations and amplitudes of those currents were selected to match the observations. It is the responses to those FACs that account for the periodic displacements of the magnetotail current sheet, the varying thickness of the nightside plasma sheet, the intensity of the rotating field-aligned currents, and the location and displacement of the magnetopause and bow shock, all of which are found in the simulation and shown to be in quantitative agreement with observations. These quantitative comparisons lead us to believe that most properties of the periodic perturbations observed in Saturn's magnetosphere are quite well modeled. It seems that the waves generated in the system have the right amplitudes and impose appropriate perturbations even on remote parts of the system, but they take a bit too long to reach large distances from their sources in the ionosphere. To summarize, it seems that at large distance, the simulation models the periodic disturbances quite well but that the phase of the rotation at which different responses develop may be inaccurate.

6. Magnetopause Asymmetries

Asymmetries of the magnetopause boundary in the equatorial plane can, in principle, arise from deviations of the flow direction of the solar wind or from a strong dawn-dusk component of the interplanetary magnetic field. However, at rapidly rotating planets such as Saturn and Jupiter, the sense of plasma rotation, sunward on the dawn flank and antisunward on the dusk flank, implies that asymmetry can be internally driven. In an investigation of the form of the magnetopause of Jupiter, *Joy et al*. [2002] identified a very weak dawn-dusk asymmetry of Jupiter's magnetopause, but studies of Saturn's magnetopause have assumed little asymmetry. *Clarke et al*. [2010a] allow a slightly asymmetric magnetopause to rock in the dawn-dusk direction about the Sun-planet line. However, our simulated magnetopause shows considerable dawn-dusk asymmetry modulated by rotational phase.

The magnetopause defined as the open-closed field line separatrix is shown at different rotation phases in Figure 1. In Figure 6a, these different traces have been superimposed. It is striking that the largest excursions of the boundary are localized on the morning side. A quadratic fit to the mean of the plotted magnetopause locations in the local time range from dawn to dusk yields (distances in Saturn radii)

$$X = -0.016\,Y^2 \;-\; 0.042\,Y + 26.61 \tag{1}$$

This fit is plotted in Figure 6b. At the terminator, the means fall at $-42.1\ R_S$ and $+39.5\ R_S$, a dawn-dusk asymmetry of 6%.

The extrema of the magnetopause displacement from the mean as a function of local time are shown in Figure 6c with maximum displacement plotted in black and minimum displacement plotted in blue. An average of these curves (in red) and a fit to the average (in green) for the local time sector between 0700 and 1700 LT

$$\text{Displacement amplitude } (R_s) = 8.64\text{–}0.47\ \text{LT(h)} \tag{2}$$

are also shown. Typical excursions near noon are close to $\pm 3\ R_S$. Near dusk they drop to ~1 R_S. Near dawn they may become as large as 9 R_S.

There is evidence in the work of *Clarke et al*. [2010a] that the asymmetry we extract from the simulation is observed. Table 2 of that paper lists 77 magnetopause encounters observed on 68 orbits. Only 15 were encountered at distances beyond the 42.1 R_S that we suggest as the mean location at 0600 LT, and they were

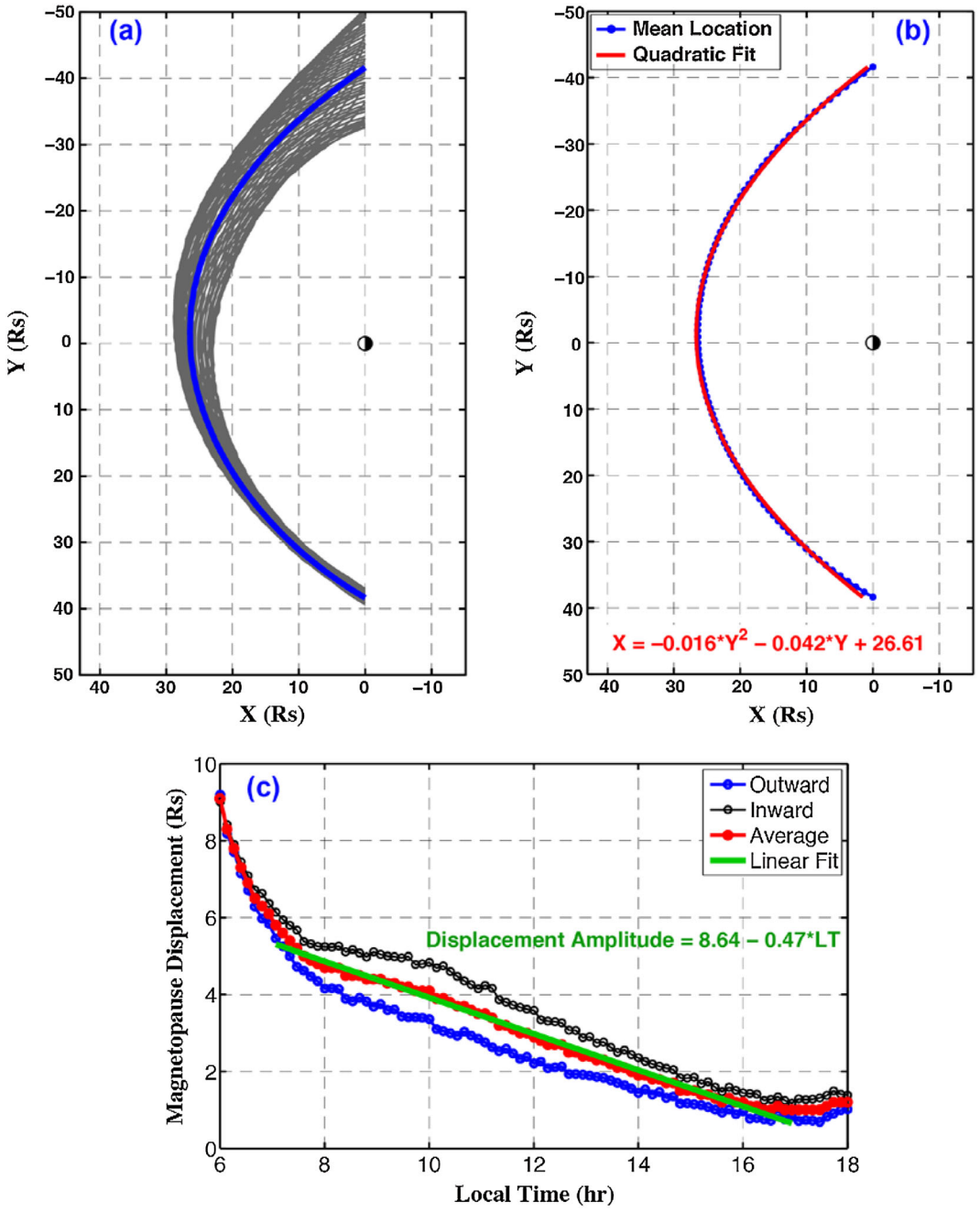

Figure 6. (a) Magnetopause boundary every 1 h through five rotation cycles (grey) and fit to the mean (blue). (b) Quadratic fit (red) to the mean magnetopause position (blue). (c) Maximum (black) and minimum (blue) magnetopause displacements from the mean radial distance versus LT, average of this displacement versus LT (red), and linear fit to the displacement versus LT (green).

all on the morning side. Our Table 1 lists properties of 21 encounters within 2 h of dawn and 8 within 2 h of dusk. The radial distances of our average model magnetopause are also listed in the table. The data and model track each other closely, and both show the strong asymmetry on which we remark.

7. Links to Other Magnetospheric Responses

The strong asymmetry of the magnetopause described in the previous section must relate to the nature of periodic flows and compressional perturbations that characterize the internally driven dynamics of the system.

Table 1. Data on Magnetopause Crossings Within 2 h of Dawn (Columns 1–4) and Dusk (Columns 5–8) Reported by *Clarke et al.* [2010a] (Ordered by Local Time) Compared With Predictions From the Simulation From Equations (1) and (2)[a]

Orbit	Local Time	$R_{Observed}$	R_{Model}	Orbit	Local Time	$R_{Observed}$	R_{Model}
21/22	4.4	44.7	60.5 ± 6.6	43/44	16.1	35.8	31.9 ± 1.1
20/21	4.4	66.5	59.9 ± 6.6	49/50	16.2	42.2	32.2 ± 1.0
17/18 out	4.6	37.3	56.6 ± 6.5	45/46	16.3	33.5	32.6 ± 1.0
A out	4.7	46.1	54.8 ± 6.4	46/47	16.6	29.3	33.7 ± 0.8
18/19	4.8	40.8	41.2 ± 6.4	44/45	16.9	29.3	35.0 ± 0.7
19/20 out	5.1	43.2	48.8 ± 6.2	47/48	17.2	39.3	36.6 ± 0.6
16/17	5.8	29.9	41.2 ± 5.9	40/41	17.6	30.4	39.1 ± 0.4
C out	5.8	44.7	41.2 ± 5.9	48/49	17.9	28.6	41.3 ± 0.2
B out	5.9	44.9	40.3 ± 5.9				
6/7 out	6.0	28.5	42.1 ± 5.8				
12/13	6.1	32.1	38.7 ± 5.8				
19/20 in	6.2	46.1	38.0 ± 5.7				
13/14	6.3	34.6	37.3 ± 5.7				
8/9	6.3	32.5	37.3 ± 5.7				
7/8	6.3	31.5	37.3 ± 5.7				
4/5 out	6.4	32.5	36.6 ± 5.6				
15/16	7.0	40.5	33.4 ± 5.4				
9/10	7.05	39.6	33.1 ± 5.3				
17/18 in	7.2	45.7	32.5 ± 5.2				
3/4 out	7.2	41.3	32.5 ± 5.2				
SOI	7.7	33.6	30.6 ± 5.0				

[a](Equation (1) has been extrapolated to times earlier than those used for the fit.) Local time in hours, distances in R_S. Multiple close encounters are calculated using averages over distances and local times on a single pass. SOI is the inbound capture orbit referred to as "Saturn Orbit Insertion."

In the *Jia et al.* [2012] and *Jia and Kivelson* [2012] simulations, major configurational changes are imposed by the rotating current system generated in the ionosphere. On each rotation cycle, a plasmoid develops in the midnight-morning quadrant and propagates dawnward, northward, and antisunward, while expanding in size (see Figure 8 of *Jia et al.* [2012]), setting up flows and distorting the surrounding plasma and field. The interplay of field and plasma perturbations directly imposed by the rotating cam current and those generated by propagating plasmoids greatly complicates the interpretation of periodic behavior in parts of the magnetosphere remote from the magnetic shell carrying the highest intensity FACs. The way in which flows related to the plasmoid release affect the structure of the system is evident from the changing configuration of the 70° invariant latitude magnetic shell on which we have commented above. We have evaluated the mass flux through quadrants of a cylinder of 20 R_S radius and height ± 10 R_S as a function of rotation phase. On each rotation cycle, peak fluxes occur successively through the quadrants centered at midnight, at dawn, and at noon; and the rotating cam linked to this outflow pushes out the magnetopause, first near dawn (Figure 1a), later near noon (Figure 1d), and with decreasing effectiveness with increasing LT to dusk. Thus, the magnetopause should not be thought of as rocking from dawn to dusk, but rather as responding to an ever weakening driver that rotates within its confinement once each rotation period. This interpretation accounts for the strong dawn and dusk asymmetry observed in both Cassini measurements and in the simulation.

8. Discussion and Summary of Testable Predictions

The MHD simulation of *Jia et al.* [2012] was designed to interpret the periodicities that appear in a wide range of magnetospheric phenomena at Saturn. The rotating magnetic perturbations of the inner magnetosphere provided evidence that a rotating system of FACs must play a central role in producing the periodic responses and that many features of the magnetosphere can be understood in terms of the perturbations imposed fairly directly by those rotating cam currents. However, other periodic features of the system such as the flapping of the tail plasma sheet and the periodic excursions of the magnetopause require that compressional forces be present. Compressional forces are transmitted by magnetosonic waves whose propagation is omnidirectional. Although rotating and propagating signals are generated by the same sources, the differences in propagation produce a distinctly nonsinusoidal response that may differ considerably from one part of the magnetosphere to another. *Ramer et al.* [2013] have emphasized that the rotational phase dependence of plasma and field properties varies with location in the magnetosphere, attributing the effect largely to the

expansion and contraction of the system. Here we have shown that the simulation launches compressional waves from the dominant southern source, and it is these waves that cause the plasma sheet to change its magnetic and plasma configuration and to flap. Propagating toward the dayside boundary, these waves produce periodic nonsinusoidal displacement of the magnetopause and the bow shock. Their effects are strongly modified by the confining forces of the dayside magnetopause, but the pressure fronts are probably significant in producing highly structured flow with a significant dawn-dusk component in the magnetotail.

We have provided quantitative descriptions of the properties of the magnetopause position and motion that we suggest are worth testing. We find that excursions of magnetopause distance about the mean are nonsinusoidal, with long dwells near the largest displacements and short-lived, deep penetrations inward, a description that may provide a useful guide for further analysis of boundary motions in Cassini data. We also find a significant dawn-dusk asymmetry, with extreme excursions about the mean on the dawnside and highly limited excursions about the mean on the duskside. Fits to the expected forms provided in equations (1) and (2) should prove helpful in studies of boundary properties.

Acknowledgments

We thank Tamas Gombosi for establishing a powerful computational framework without which this work could not have been undertaken. We are also grateful to David Southwood for useful discussions on the subject. This work was supported by NASA through grants NNX12AK34G at the University of Michigan (X.J. and M.G.K.) and NNX10AF16G at UCLA (M.G.K.) and by the Cassini mission under contracts JPL 1409449 (X.J.) and 1416974 (M.G.K.). Data used in this study were obtained from simulations using the SWMF/BATSRUS code developed at the University of Michigan, which is available at http://csem.engin.umich.edu/tools/swmf/. The simulation run presented in this study was performed on the Pleiades supercomputer managed by the NASA Advanced Supercomputing Division.

M.A. Balikhin thanks two anonymous reviewers for their assistance in evaluating this paper.

References

Andrews, D. J., E. J. Bunce, S. W. H. Cowley, M. K. Dougherty, G. Provan, and D. J. Southwood (2008), Planetary period oscillations in Saturn's magnetosphere: Phase relation of equatorial magnetic field oscillations and Saturn kilometric radiation modulation, *J. Geophys. Res.*, *113*, A09205, doi:10.1029/2007JA012937.

Andrews, D. J., S. W. H. Cowley, M. K. Dougherty, and G. Provan (2010a), Magnetic field oscillations near the planetary period in Saturn's equatorial magnetosphere: Variation of amplitude and phase with radial distance and local time, *J. Geophys. Res.*, *115*, A04212, doi:10.1029/2009JA014729.

Andrews, D. J., A. J. Coates, S. W. H. Cowley, M. K. Dougherty, L. Lamy, G. Provan, and P. Zarka (2010b), Magnetospheric period oscillations at Saturn: Comparison of equatorial and high-latitude magnetic field periods with north and south Saturn kilometric radiation periods, *J. Geophys. Res.*, *115*, A12252, doi:10.1029/2010JA015666.

Arridge, C. S., et al. (2011), Periodic motion of Saturn's nightside plasma sheet, *J. Geophys. Res.*, *116*, A11205, doi:10.1029/2011JA016827.

Carbary, J. F. (2013), Longitude dependences of Saturn's ultraviolet aurora, *Geophys. Res. Lett.*, *40*, 1902–1906, doi:10.1002/grl.50430.

Carbary, J. F., D. G. Mitchell, P. Brandt, C. Paranicas, and S. M. Krimigis (2008), ENA periodicities at Saturn, *Geophys. Res. Lett.*, *35*, L07102, doi:10.1029/2008GL033230.

Clarke, K. E., et al. (2006), Cassini observations of planetary-period oscillations of Saturn's magnetopause, *Geophys. Res. Lett.*, *33*, L23104, doi:10.1029/2006GL027821.

Clarke, K. E., D. J. Andrews, C. S. Arridge, A. J. Coates, and S. W. H. Cowley (2010a), Magnetopause oscillations near the planetary period at Saturn: Occurrence, phase, and amplitude, *J. Geophys. Res.*, *115*, A08209, doi:10.1029/2009JA014745.

Clarke, K. E., D. J. Andrews, A. J. Coates, S. W. H. Cowley, and A. Masters (2010b), Magnetospheric period oscillations of Saturn's bow shock, *J. Geophys. Res.*, *115*, A05202, doi:10.1029/2009JA015164.

Desch, M. D., and M. L. Kaiser (1981), Voyager measurement the rotation rate of Saturn's magnetic field, *Geophys. Res. Lett.*, *8*(3), 253–256, doi:10.1029/GL008i003p00253.

Gurnett, D. A., et al. (2005), Radio and plasma wave observations at Saturn from Cassini's approach and first orbit, *Science*, *307*, 1255–1259, doi:10.1126/science.1105356.

Gurnett, D. A., A. M. Persoon, W. S. Kurth, J. B. Groene, T. F. Averkamp, M. K. Dougherty, and D. J. Southwood (2007), The variable rotation period of the inner region of Saturn's plasma disk, *Science*, *316*, 442–445, doi:10.1126/science.1138562.

Jia, X., and M. G. Kivelson (2012), Driving Saturn's magnetospheric periodicities from the upper atmosphere/ionosphere: Magnetotail response to dual sources, *J. Geophys. Res.*, *117*, A11219, doi:10.1029/2012JA018183.

Jia, X., M. G. Kivelson, and T. I. Gombosi (2012), Driving Saturn's magnetospheric periodicities from the upper atmosphere/ionosphere, *J. Geophys. Res.*, *117*, A04215, doi:10.1029/2011JA017367.

Joy, S. P., M. G. Kivelson, R. J. Walker, K. K. Khurana, C. T. Russell, and T. Ogino (2002), Probabilistic models of the Jovian magnetopause and bow shock locations, *J. Geophys. Res.*, *107*(A10), 1309, doi:10.1029/2001JA009146.

Khurana, K. K., D. G. Mitchell, C. S. Arridge, M. K. Dougherty, C. T. Russell, C. Paranicas, N. Krupp, and A. J. Coates (2009), Sources of rotational signals in Saturn's magnetosphere, *J. Geophys. Res.*, *114*, A02211, doi:10.1029/2008JA013312.

Kurth, W. S., A. Lecacheux, T. F. Averkamp, J. B. Groene, and D. A. Gurnett (2007), A Saturnian longitude system based on a variable kilometric radiation period, *Geophys. Res. Lett.*, *34*, L02201, doi:10.1029/2006GL028336

Kurth, W. S., T. F. Averkamp, D. A. Gurnett, J. B. Groene, and A. Lecacheux (2008), An update to a Saturnian longitude system based on kilometric radio emissions, *J. Geophys. Res.*, *113*, A05222, doi:10.1029/2007JA012861.

Lamy, L. (2011), Variability of southern and northern SKR periodicities, in *Planetary Radio Emissions*, vol. VII, edited by H. O. Rucker et al., pp. 38–50, Austrian Academy of Science Press, Vienna.

Nichols, J. D., J. T. Clarke, S. W. H. Cowley, J. Duval, A. J. Farmer, J.-C. Gérard, D. Grodent, and S. Wannawichian (2008), Oscillation of Saturn's southern auroral oval, *J. Geophys. Res.*, *113*, A11205, doi:10.1029/2008JA013444.

Nichols, J. D., S. W. H. Cowley, and L. Lamy (2010), Dawn-dusk oscillation of Saturn's conjugate auroral ovals, *Geophys. Res. Lett.*, *37*, L24102, doi:10.1029/2010GL045818.

Paranicas, C., D. G. Mitchell, E. C. Roelof, P. C. Brandt, D. J. Williams, S. M. Krimigis, and B. H. Mauk (2005), Periodic intensity variations in global ENA images of Saturn, *Geophys. Res. Lett.*, *32*, L21101, doi:10.1029/2005GL023656.

Provan, G., S. W. H. Cowley, and J. D. Nichols (2009), Phase relation of oscillations near the planetary period of Saturn's auroral oval and the equatorial magnetospheric magnetic field, *J. Geophys. Res.*, *114*, A04205, doi:10.1029/2008JA013988.

Ramer, K. M., M. G. Kivelson, N. Sergis, K. K. Khurana, X. Jia, and R. J. Walker (2013), Spinning, breathing and flapping: Periodicities in Saturn's middle magnetosphere, *Abstract SM21A-2134*, 2013 Fall meeting of AGU, San Francisco, Calif.

Sergis, N., et al. (2010), Particle pressure, inertial force, and ring current density profiles in the magnetosphere of Saturn, based on Cassini measurements, *Geophys. Res. Lett.*, *37*, L02102, doi:10.1029/2009GL041920.

Smith, C. G. A. (2006), Periodic modulation of gas giant magnetospheres by the neutral upper atmosphere, *Ann. Geophys.*, *24*, 2709–2717.
Smith, C. G. A. (2010), A Saturnian cam current system driven by asymmetric thermospheric heating, *Mon. Not. R. Astron. Soc.*, *410*, 2315–2328, doi:10.1111/j.1365-2966.2010.17602.
Southwood, D. J., and M. G. Kivelson (2007), Saturnian magnetospheric dynamics: Elucidation of a camshaft model, *J. Geophys. Res.*, *112*, A12222, doi:10.1029/2007JA012254.
Southwood, D. J., and S. W. H. Cowley (2014), The origin of Saturn's magnetic periodicities: Northern and southern current systems, *J. Geophys. Res. Space Physics*, *119*, 1563–1571, doi:10.1002/2013JA019632.